Available online at www.sciencedirect.com
SCIENCE DIRECT®
Geomorphology 56 (2003) 49–64
GEOMORPHOLOGY
www.elsevier.com/locate/geomorph

Comparison of three GIS-based models for predicting rockfall runout zones at a regional scale

Luuk K.A. Dorren*, Arie C. Seijmonsbergen

Institute for Biodiversity and Ecosystem Dynamics—Physical Geography, Universiteit van Amsterdam, Nieuwe Achtergracht 166, Amsterdam NL-1018WV, The Netherlands

Received 2 January 2002; received in revised form 20 December 2002; accepted 23 December 2002

Abstract

Site-specific information about the level of protection that mountain forests provide is often not available for large regions. Information regarding rockfalls is especially scarce. The most efficient way to obtain information about rockfall activity and the efficacy of protection forests at a regional scale is to use a simulation model. At present, it is still unknown which forest parameters could be incorporated best in such models. Therefore, the purpose of this study was to test and evaluate a model for rockfall assessment at a regional scale in which simple forest stand parameters, such as the number of trees per hectare and the diameter at breast height, are incorporated. Therefore, a newly developed Geographical Information System (GIS)-based distributed model is compared with two existing rockfall models. The developed model is the only model that calculates the rockfall velocity on the basis of energy loss due to collisions with trees and on the soil surface. The two existing models calculate energy loss over the distance between two cell centres, while the newly developed model is able to calculate multiple bounces within a pixel. The patterns of rockfall runout zones produced by the three models are compared with patterns of rockfall deposits derived from geomorphological field maps. Furthermore, the rockfall velocities modelled by the three models are compared. It is found that the models produced rockfall runout zone maps with rather similar accuracies. However, the developed model performs best on forested hillslopes and it also produces velocities that match best with field estimates on both forested and nonforested hillslopes irrespective of the slope gradient.

Keywords: Rockfall; GIS; Protection forest; Simulation model; Geomorphological mapping; Mountainous catchment

1. Introduction

Mountain forests provide multiple functions, of which protection against rockfall, snow avalanches, and soil erosion is increasingly considered to be the most important one (Kräuchi et al., 2000; Motta and Haudemand, 2000). However, site-specific information about the level of the protection that forests provide is often not available for large regions. Information about the level of protection that mountain forests provide against rockfall is especially scarce (Meißl, 1998). Although for some known active rockfall slopes within a forest management area some qualitative information about the efficacy of the protection forest stand might be available, forest

* Corresponding author. Tel.: +31-20-5257420; fax: +31-20-5257431.
E-mail address: l.dorren@science.uva.nl (L.K.A. Dorren).

0169-555X/$ - see front matter © 2003 Elsevier Science B.V. All rights reserved.
doi:10.1016/S0169-555X(03)00045-X

departments indicate that there is a need for information on both rockfall activity and the efficacy of protection forests for whole management areas. This is because protection forest management plans and strategies aiming at the maintenance of stable forest structures are developed for large management areas and not for individual slopes (Keller, 1994; Bebi et al., 2001).

The most efficient way to obtain information about rockfall activity and the efficacy of protection forests at a regional scale is to use a simulation model (Dorren, 2003). With respect to rockfall modelling, it is known how to simulate rockfall runout zones (in this study defined as the zone between the start and the end location for a falling rock) at a slope scale (Kirkby and Statham, 1975; Bozzolo and Pamini, 1986; Pfeiffer and Bowen, 1989; Azzoni et al., 1995; Okura et al., 2000). Some authors modelled patterns of rockfall runout zones at a regional scale (van Dijke and van Westen, 1990; Meißl, 1998, 2001). All these regional models did not, however, incorporate specific protection forests parameters. Moreover, both existing regional rockfall models use a relatively simple modelling approach. Therefore, the objective of this study was to determine if the newly developed process-based rockfall model, which incorporates protection forest parameters and the effect of forest density on the velocity of falling rocks, improves the accuracy of simulated patterns of rockfall runout zones at a regional scale. To achieve this objective, this study compared the results of the newly developed model with the outcomes of the two existing Geographical Information System (GIS)-based models. To evaluate the performance of the three models, firstly, the modelled patterns of rockfall runout zones were compared with mapped patterns. Secondly, the velocities produced by the three models were analysed. For both the pattern and the velocity analysis, a distinction was made between model performance on forested and nonforested hillslopes.

2. Study area

2.1. General description

The research area covers the Montafon region, located in the southern part of Vorarlberg, the westernmost province of Austria. The Montafon region comprises the headwaters of the river Ill and covers an area of 533 km^2 mountainous terrain. Altitudes in the Montafon region vary from 580 m a.s.l. near Lorüns up to 3312 m a.s.l. at the top of the Piz Buin, which is the highest peak in the Montafon region (Fig. 1). Within the Montafon region, 50% of the area is covered by alpine meadows, 23% are forests, 20% are alpine tundra, and 7% are agricultural and urban lands. The distribution of forest stand types at a regional scale is determined mainly by altitude, but at a slope scale, other factors such as parent material, relief, microclimate, humus forms, light, and disturbances caused by natural hazards also become important (van Noord, 1996). Generally, the canopy density decreases with increasing altitude due to the changing climatic conditions (e.g., heavier snow loads). Because uneven-aged forests predominate, tree distribution, stem density, tree height, and basal area vary strongly between forest stands. As typical for mountain forests, these varied forest stands are distributed in a patchy mosaic-like structure (Maier, 1993). Mixed forests predominate in the montane zone (500–1200 m a.s.l.) and coniferous forests (mainly *Picea abies*) in the subalpine zone (1200–1900 m a.s.l.).

The climate in the Montafon region is of the central European type with seasonal rainfall regime producing a winter minimum and a summer maximum. Since the mountainous topography determines the local climate, it may be classified as Df according to the Köppen climate system (Köppen, 1918). The average winter temperature lies between 0 and −5 °C and the average summer temperature between 7 and 17 °C. Annual precipitation varies between 1200 and 1700 mm (source: Vorarlberger Illwerke, Schruns). Both temperature and precipitation vary strongly with altitude and aspect. Föhn winds are important in the lower part of the Montafon region. The total yearly evaporation varies between 250 and 400 mm (i.e., approximately 25% of the precipitation).

2.2. Geology and geomorphology

The geological structure of the Montafon region is dominated by the Alpine orogeny, during which several large overturned folds or nappes were overthrust from a south-eastern direction. The two largest

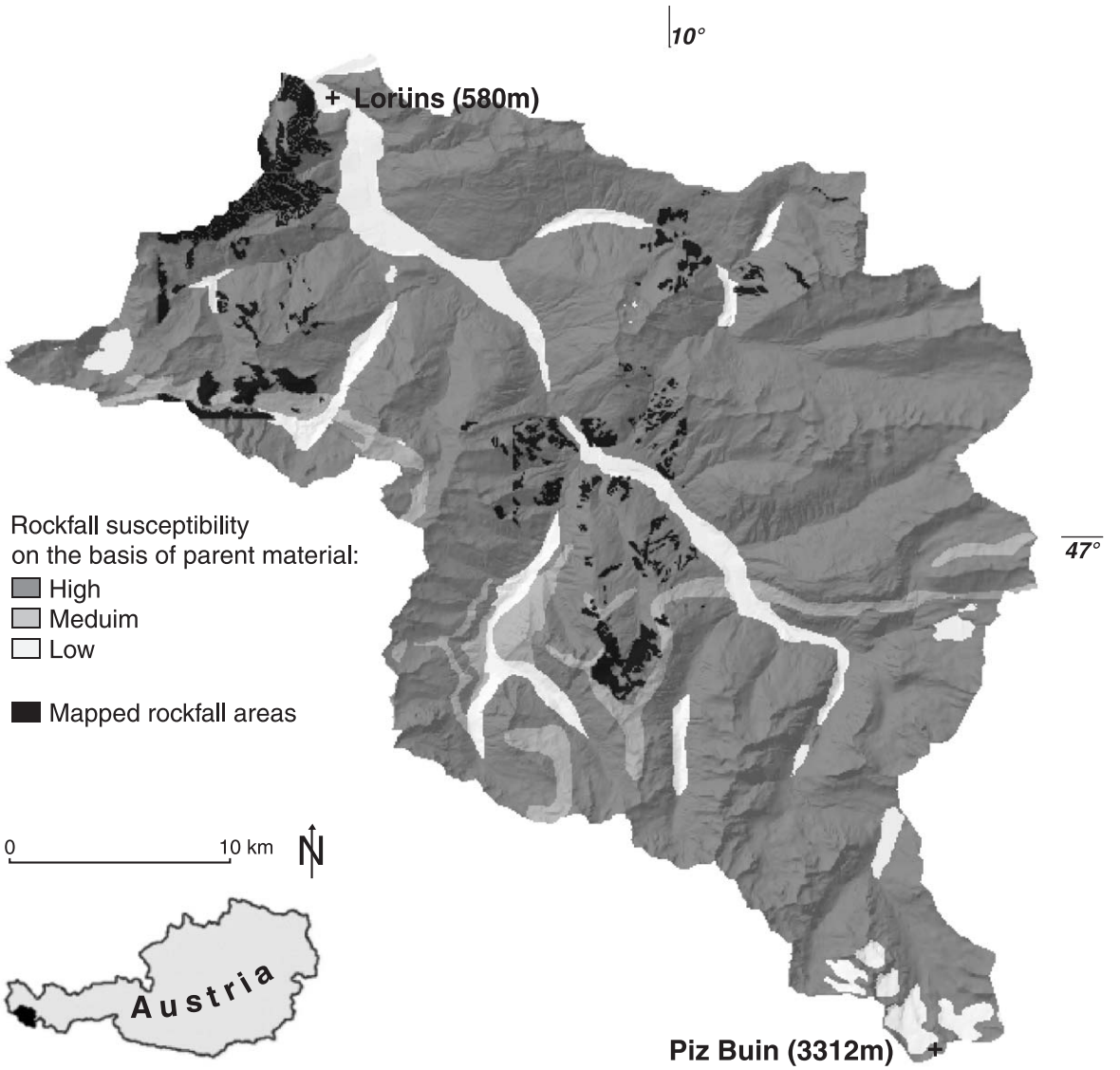

Fig. 1. Map showing the rockfall susceptibility map on the basis of parent material or bedrock type throughout the Montafon region. The black areas indicate mapped active rockfall areas.

and most important nappes are the Silvretta nappe in the southeastern and the Lechtal nappe in the northwestern part of the study area, which are both Upper East Alpine nappes (GBA, 1998). The Silvretta nappe consists of crystalline formations and the Lechtal nappe consists of resistant limestones and dolomites. The crystalline formations consist mainly of metamorphic rocks, especially paragneisses, but in the most southeastern part of the Silvretta nappe, orthogneisses and granites dominate. The transition zone between the crystalline and the sedimentary formations is known as the 'Phyllitgneis zone.'

The Pleistocene glacial and interglacial periods have had a profound impact on the landscape: firstly, in terms of the production and redistribution of loose materials, and secondly, because of pronounced glacial erosion, which resulted in oversteepened slopes. Postglacial relaxation of these slopes led to the

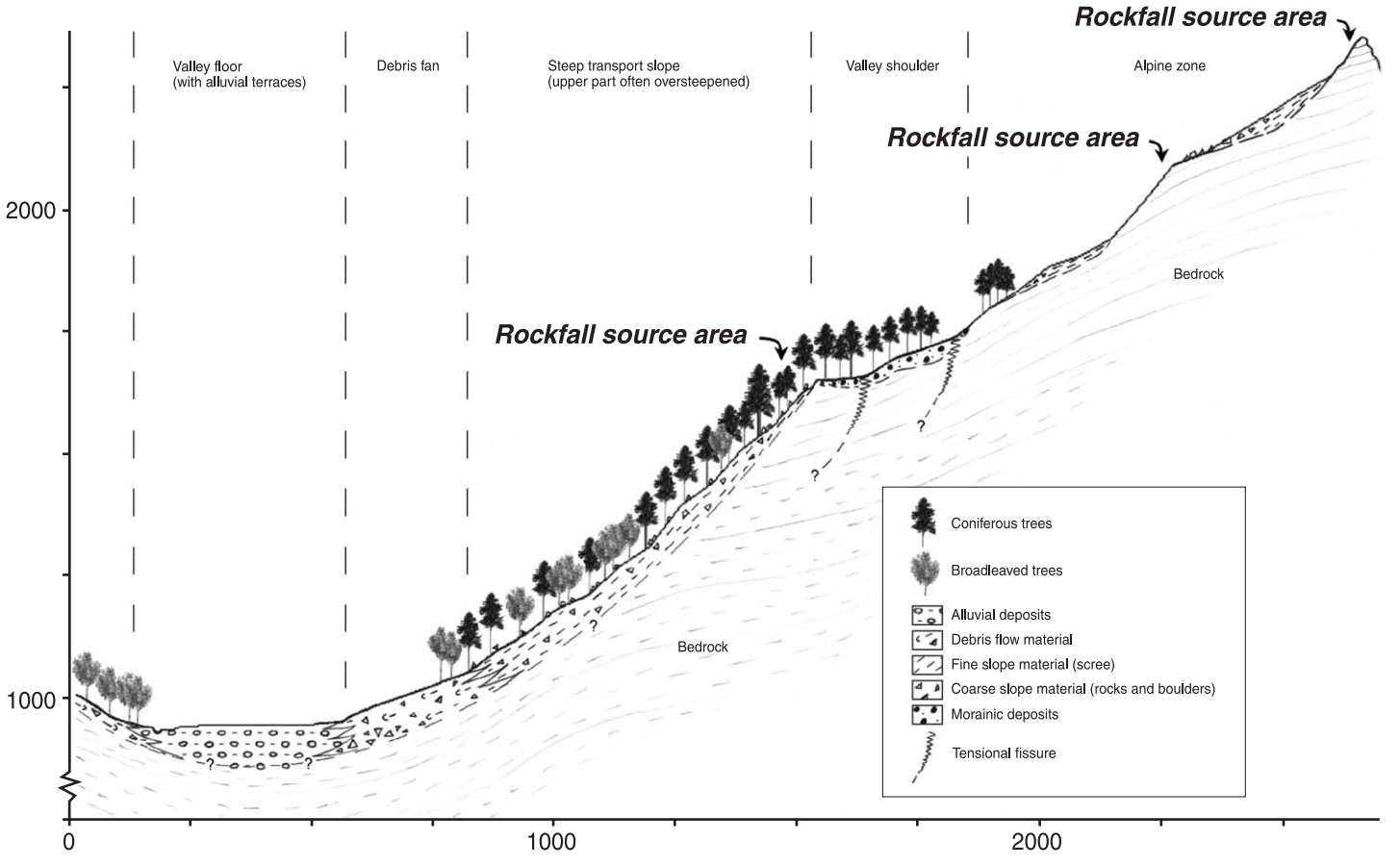

Fig. 2. General characterization of a typical slope transect in the Montafon region with deposits and rockfall source areas, showing an exaggerated vertical scale for the trees and the thickness of nonlithified materials. Question marks indicate uncertainty about the depth of boundaries or the depth of fissures. The structural layering of the bedrock is variable throughout the region (after van Noord, 1996).

development of tensional fissures and related deep-seated mass movements, bedrock toppling, as well as landsliding (van Noord, 1996). This Quaternary development, in combination with the geological structure, sets the initial conditions for the development of rockfall source areas throughout the region (Fig. 2).

In general, present rockfall source areas are found in two zones. Firstly, they are found above the steep transport slope below the valley shoulder, and secondly, in the alpine zone above the timberline (Fig. 2). Obstacles like dead wood, tree stems, shrubs, and boulders act as barriers against falling rocks on the steep transport slope. In the alpine zone, falling rocks decelerate due to the decreasing slope gradient at the bottom part of talus slopes, but also due to the increasing surface roughness produced by larger rocks (Statham and Francis, 1986).

3. Materials

A digital elevation model (DEM) produced by the National Austrian Mapping Agency was available for this study (BEV, 2001). This DEM was arranged as a regular grid of surface height measurements with a spacing of 25 m. From this DEM, a map with mean slope gradients was derived using the method of Zevenbergen and Thorne (1987). Also available were a geological map and a digital land-cover map. The 1:200,000 geological map of the Province of Vorarlberg (GBA, 1998) provided information on the main formations and tectonic units. This map was digitised, labelled, and converted to a raster with a cell size of 25×25 m (1421 rows and 1437 columns, similar to the DEM). Subsequently, the prevailing rock types and the estimated rockfall susceptibility as well as the mean rock density (GSC, 2002) were added to the geological GIS map for each formation as well (Table 1). The estimated rockfall susceptibility data have been used to create Fig. 1.

This digital land-cover map was derived from a September 1998 Landsat TM image using a maximum likelihood classification for the land-cover classes: bare, lakes, snow/ice, alpine meadows and shrubs, valley meadows, and forest. Subsequently, the forested areas have been reclassified in the classes: broadleaved forest, mixed forest, dense coniferous forest, and open coniferous forest. This was done with an object-based classification technique (see Dorren et al., in press). After classification, we refined the land-cover classes on the basis of slope classes provided by the DEM. This resulted in the final land-cover classes: cliff face (60–90°), steep bare slope (40–60°), scree slope (30–40°), bare slope (0–30°), meadow, alpine shrubs, bushes, broadleaved forest, mixed forest, dense coniferous forest, and open coniferous forest. In addition, the attributes DBH (stem diameter at breast height, normally measured at ~ 1.3 m at the upslope side) and the average number of trees per hectare were added to the forest classes in the land-cover map. These attributes were derived from the most recent regional forest inventory, which treated existing forest compartments as homogeneous (Maier,

Table 1
Data on the different rock types and materials used in the model (based on GSC, 2002)

Rock types	Formation/tectonic unit	Rock density [kg/m^3]	Rockfall susceptibility
Slate, marl, and sandstone	'Praetigau' flysch—'Gempi' slice	2400	Low
Limestone, sandstone, and schist	'Falknis' nappe	2600	Medium
Limestone	'Sulzfluh' nappe	2500	High
Chert and marl	'Arosa' zone	2400	Low
Limestone (Muschelkalk) and dolomite	Sediment of the 'Geisberg' area	2600	High
Gneiss, amphibolite, and limestone	'Madrisa' zone	2900	High
Dolomite and limestone	'Lechtal' nappe	2400	High
Amphibolite, ophiolite, and gneiss	'Silvretta' nappe	2950	High
Quartzite-bearing gneiss and granite gneiss	'Silvretta' nappe	2750	High
Mica schist	'Silvretta' nappe	2750	Low
Biotite-bearing gneiss	'Silvretta' nappe	2650	High
Serpentine, calcite, and amphibolite	Ophiolites in the Penninic zone	3000	High

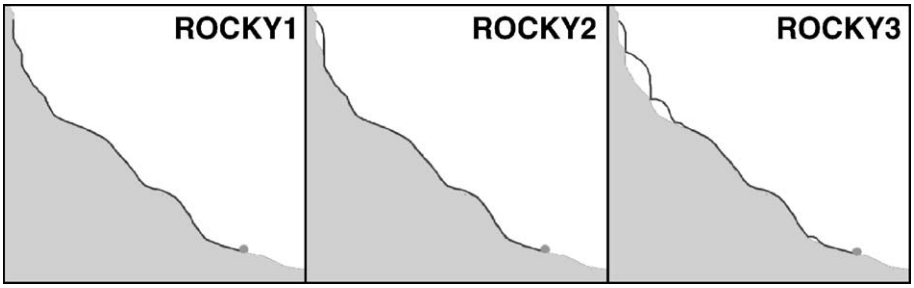

Fig. 3. Simple 2D representations of the different approaches of the three models tested: ROCKY1 only simulates sliding; ROCKY2 simulates initial freefall and then sliding; and ROCKY3 simulates sequences of bounces and motion through the air.

1993). A forest compartment is an area that is managed as a unit because of geoecological or ownership boundaries; a forest compartment may include multiple forest stands.

The dataset was completed by geomorphological raster maps, which were derived from digitised 1:10,000 geomorphological field maps (Fig. 3). The field mapping was based on a system described by De Graaff et al. (1987) and Seijmonsbergen (1992). These maps were coloured line symbol maps and incorporated information on drainage, morphography/morphometry, nonlithified materials, genesis of landforms, and current geomorphological processes (Seijmonsbergen, 1992). The information on the distribution and activity of rockfall areas in the study area derived from these maps served as a control. The rockfall areas were defined as cliff faces with scree slope below. The relative activity could be estimated by identifying the freshness of the scree. Approximately 20% of the study area was mapped using this mapping system. Some of these maps were completed recently, whereas the older ones were checked in the field on their accuracy regarding the information on distribution and activity of rockfall areas.

4. Models and methods

Three rockfall models were programmed in MATLAB 5.3 (Mathworks, 2002). Input data for the models were provided by raster analyses in the GIS Arcview 3.2 (ESRI, 2002). The first rockfall model (ROCKY1) is based on the algorithms described by Scheidegger (1975) and van Dijke and van Westen (1990). The second rockfall model (ROCKY2) forms an extended version of ROCKY1 and is based on the *Sturzgeschwindigkeit* model developed by Meißl (1998). The third rockfall model (ROCKY3) is based on algorithms modified from Pfeiffer and Bowen (1989). The main difference between ROCKY3 and the other two models is that ROCKY3 is able to simulate multiple bounces of a falling rock within a pixel. The other two models calculate the velocity of the rock on the basis of one calculation between two cell centres. The following paragraphs describe how each model calculates the source areas, the fall direction, and the runout zones of simulated falling rocks.

4.1. Source area and falltrack calculation

Potential rockfall source areas were determined on the basis of the mean slope gradient map and the geological map. Areas such as morainic and scree slopes, lake, rivers, glaciers, and floodplains were disqualified as potential rockfall source areas. Those areas or cells with both a mean slope gradient equal to or greater than 40° and which were classified as bedrock according to the geological map were considered as potential rockfall source areas or source cells. From these source cells, rocks were simulated as falling from vertical cliff faces with a height of 10 m. The initial vertical velocity of the rock was − 1 m/s (negative direction is downslope) and the initial horizontal velocity was 1 m/s (positive is normal to the slope surface).

The fall direction from each raster cell is defined as the direction of the steepest descent towards a neighbouring cell. The steepest descent is calculated as the change in height between two cells divided by the distance between the cell centres. This method is

based on deriving flow direction from a DEM presented in Jenson and Domingue (1988). The three models tested all applied the above-described procedures.

4.2. Runout zone calculation

The length of each rockfall runout zone is calculated on the basis of the velocity of a falling rock. In general, a falling rock starts with acceleration on the steeper slope parts and decelerates on slope parts with lower mean slope gradient until it stops in a certain position, depending on the vegetation cover and slope surface properties.

ROCKY1 calculates the velocity on the basis of energy conservation of a mass that is considered to slide over a slope surface (Fig. 4) as defined by Scheidegger (1975). In this energy conservation approach, a friction coefficient was responsible for energy loss. For each cell in the falltrack, the velocity of the falling rock was calculated as follows:

$$V_{out} = \sqrt{V_{in}^2 + 2g(h - \mu + X)} \quad (1)$$

where: V_{out} = outgoing velocity [m/s]; V_{in} = incoming velocity [m/s]; $g = 9.81$ [m/s^2]; h = fall height [m] (height difference between two raster cells); μ = friction coefficient [−]; and X = horizontal fall distance [m].

This velocity is calculated for each cell within the falltrack, starting at the rockfall source cell. The value of the friction coefficient depends on the surface cover characteristics, including the plasticity of the material

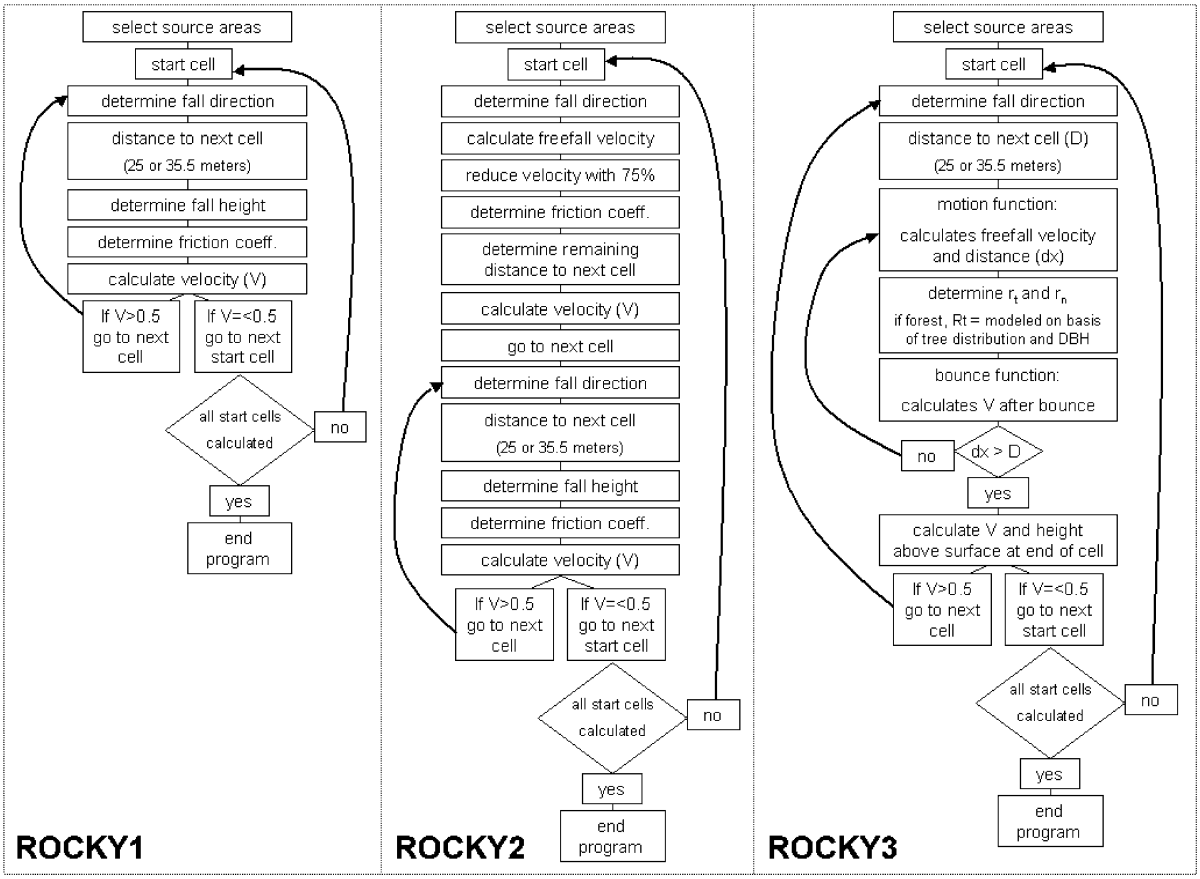

Fig. 4. Flow diagrams presenting a general overview of the three models tested.

covering the slope and the obstacles on the slope surface like vegetation, rocks, and dead wood. Values for the friction coefficient have been derived from literature (van Dijke and van Westen, 1990; Meißl, 1998) and are presented in Table 2.

ROCKY2 is quite similar to ROCKY1, except for the initial velocity calculation. In this model, the falling rock is considered to fall through the air, before it slides over the slope surface (Fig. 4). ROCKY2 calculates motion through the air with an idealized model (representing the rock as a single particle with a certain radius), and accelerates due to gravity, without incorporating the effect of air resistance. To account for energy loss during the first collision or bounce on the slope surface, 75% of the velocity gained during the motion through the air is subtracted. In the following cells, the velocity is calculated using Eq. (1).

ROCKY3 simulates a falling rock by sequences of bouncing and motions through the air (Fig. 4). Several of these sequences can occur within a pixel. The calculation of the motion through the air is similar to ROCKY2, using standard algorithms for describing a parabolic flight of a uniform accelerating particle. To calculate the velocity after the bounce, the velocity before a bounce is resolved into a tangential velocity (Vt_{in}, parallel to the slope surface) and a normal velocity (Vn_{in}, perpendicular to the slope surface).

Table 2
Tangential and normal coefficients of restitution (r_t and r_n, respectively) and the coefficient of friction (μ) used for the different land-cover types defined in this study

Land cover	r_t	r_n	μ
Cliff face (60–90°)	0.95	0.45	0.25
Steep bare slope (40–60°)	0.90	0.40	0.45
Scree slope (30–40°)	0.88	0.32	0.60
Bare slope (0–30°)	0.87	0.35	0.50
Meadow	0.87	0.30	0.55
Alpine shrubs	0.85	0.30	0.60
Bushes	0.83	0.30	0.65
Forest (200 trees per hectare average)	0.01–0.85[a] (mean 0.67)	0.28	1.00
Forest (300 trees per hectare average)	0.01–0.85[a] (mean 0.57)	0.28	1.50
Forest (500 trees per hectare average)	0.01–0.85[a] (mean 0.38)	0.28	2.00
Forest (700 trees per hectare average)	0.01–0.85[a] (mean 0.27)	0.28	2.20

[a] The distribution is dependent on the number of trees per hectare (see text for explanation).

The tangential velocity after a bounce is calculated with:

$$Vt_{out} = \sqrt{\frac{R^2(I\omega^2 + MVt_{in}^2)r_t}{(I + MR^2)}} \quad (2)$$

where: Vt_{out} = tangential velocity after the bounce [m/s]; R = radius of the falling rock [m]; I = moment of inertia = $2/5MR^2$ [kg m^2]; ω = rotational velocity [rad/s] = Vt_{out}/R; M = mass of the falling rock [kg]; Vt_{in} = tangential velocity before the bounce [m/s]; and r_t = tangential restitution coefficient determining energy loss [−].

The normal velocity after a bounce is calculated with:

$$Vn_{out} = Vn_{in}r_n \quad (3)$$

where: Vn_{out} = normal velocity after the bounce [m/s]; Vn_{in} = normal velocity before the bounce [m/s]; and r_n = normal restitution coefficient determining energy loss [−].

During every bounce within a pixel, ROCKY3 reduces the slope angle with a random value between 0° and 4°, as shown in Fig. 5. This procedure was programmed to account for the slope variability in the field, since slopes with perfectly straight slopes over a horizontal distance of 25 m hardly exist. We only allow the model to decrease the mean slope gradient during a bounce since rocks tend to bounce on the flatter parts of a scree slope. Rocks lying on the side with the two largest axes mainly form these slopes. This procedure was similar to the varying impact angle based on the surface roughness as described by Pfeiffer and Bowen (1989).

If the horizontal distance travelled by a rock between two bounces modelled in ROCKY3 is less than its diameter, the rock is considered to be rolling. Then the rock will be given a new displacement over the slope surface equal to the diameter of the rock. This prevents an infinite amount of simulated bounces per raster cell (after Pfeiffer and Bowen, 1989). Sequences of motion through the air followed by a bounce are repeated until the velocity of the falling rock is equal to or less than 0.5 m/s. This limit is also used for calculating the end location of the rockfall runout zones in ROCKY1 and ROCKY2. The flow diagrams presented in Fig. 6 visualize the different simulation steps for the tested models.

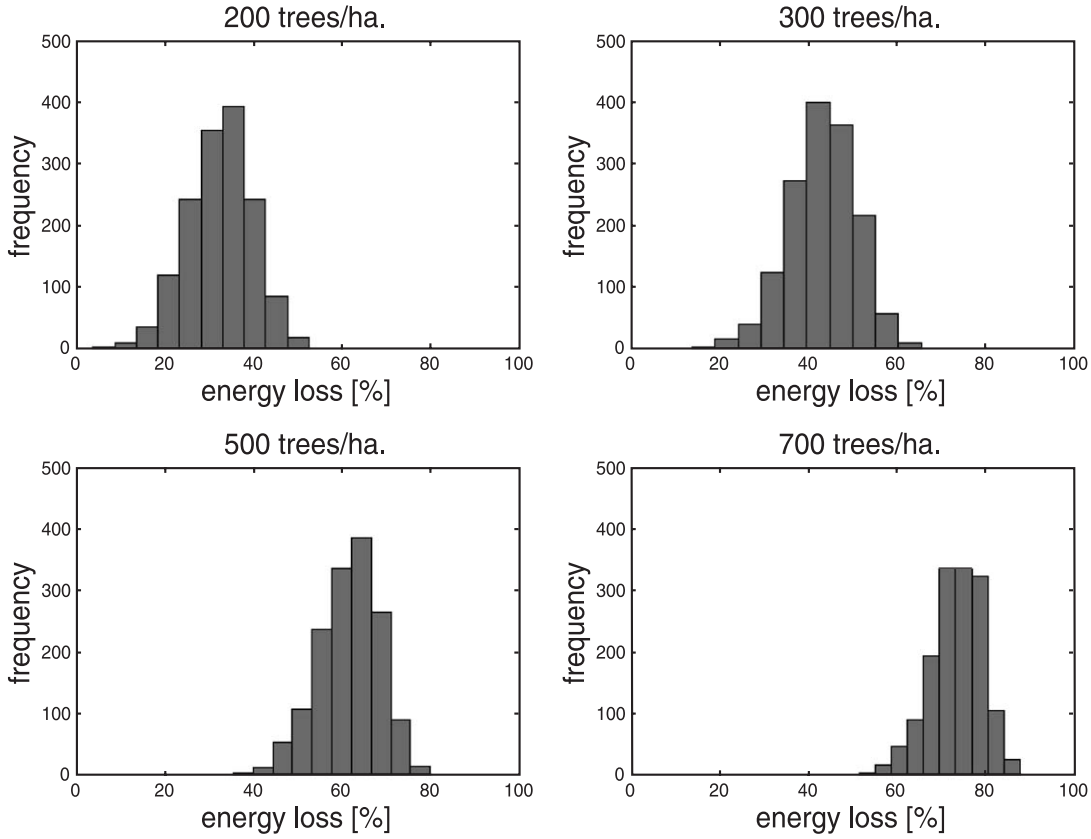

Fig. 5. Histograms of energy loss within a pixel for 200, 300, 500, and 700 trees per hectare.

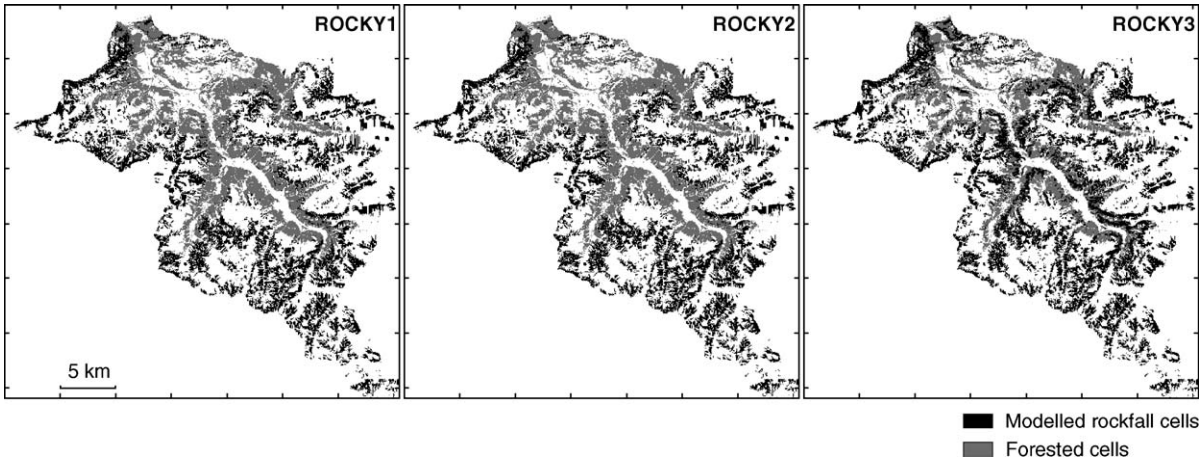

Fig. 6. Modelled patterns of rockfall runout zones within the study area produced by the three models.

4.3. Estimating input parameter values

In addition to the mean slope gradient, the determining parameter for the length of rockfall runout zones in ROCKY1 and ROCKY2 is the friction coefficient. In ROCKY3, this is the tangential and the normal restitution coefficient. These parameters represent surface cover and soil characteristics, which determine the amount of energy loss during each bounce. The friction coefficient, the tangential restitution coefficient, and the normal restitution coefficient were not calibrated on the basis of data that were measured throughout the study area. Instead, these model parameters were estimated on the basis of the land-cover map in combination with published data (Pfeiffer and Bowen, 1989; van Dijke and van Westen, 1990; Kobayashi et al., 1990; Giani, 1992; Azzoni et al., 1995; Chau et al., 1998, 2002; Meißl, 1998). The parameter values used in this study are shown in Table 2.

Estimating the tangential restitution coefficient on forested slopes was a special case. In every raster cell classified as forested, ROCKY3 simulated a forest density based on the number of trees per hectare and the DBH given for that particular cell. Within ROCKY3, a module that distributes trees randomly in a 25 × 25-m cell and calculates the energy loss as a result of different collisions with tree stems was programmed. The rock is being modelled as falling through the centreline or the diagonal of the raster cell, depending on the fall direction. In addition, the positions of the tree stems in the cell are known. This allows the model to calculate the position of the rock with respect to the tree stem during each simulation step. Since data on energy loss of falling rocks due to impacts on tree stems were not available, the following equation is used to estimate energy losses:

$$\Delta E = \sqrt{1 - \left(\frac{d}{0.5\mathrm{DBH} + R}\right)^2} \qquad (4)$$

where: ΔE = fraction of energy loss due to an impact against a tree stem [−]; d = distance between the centre of the rock and the centre of the tree stem [m]; DBH = diameter of the tree stem at breast height [m]; and R = radius of the falling rock [m].

We developed this formula assuming that a tree stem absorbs a maximum amount of kinetic energy if a central collision between a rock and a tree stem occurs. In reality, falling rocks could collide with trees at a certain height above the surface. Subsequently, a rock falls on the ground and gains new kinetic energy. This process is incorporated in the model by limiting the maximum energy loss to 99%. After the energy loss is calculated, the translation energy and the rotation energy are multiplied by the calculated fraction of energy loss. Subsequently, the resulting energies are transformed into a resultant velocity. If a rock does not collide against a tree stem, a bounce is simulated with a tangential coefficient of restitution of 0.87.

Apart from the model tests carried out with ROCKY3 for the whole study area, simulations of rocks falling through a single pixel were carried out using 1500 different tree distributions with 200, 300, and 500 trees per hectare as well as the extreme value of 700 trees per hectare. The preliminary outcomes of these simulations provided histograms of energy loss per class of number of trees per hectare (Fig. 5).

4.4. Model comparison

The radius of the simulated rocks in all the models tested was 0.25 m. This radius was used to calculate the weights of the falling rocks on the basis of the densities presented in Table 1. The modelled patterns of rockfall runout zones produced by the three models will be compared with the patterns of rockfall deposits derived from the geomorphological field maps. For this comparison, contingency tables are used. From these tables, the overall accuracies normalized for the number of mapped rockfall cells are calculated. In

Table 3
Summarized results of the tested models

	ROCKY1	ROCKY2	ROCKY3
Correctly modelled rockfall cells on forested slopes [%]	9.5	6.3	54.4
Correctly modelled rockfall cells on nonforested slopes [%]	67.4	67.4	66.8
Matches on forested slopes (nonrockfall and rockfall) [%]	53.7	52.5	66.9
Matches on nonforested slopes (nonrockfall and rockfall) [%]	75.5	75.4	75.4
Normalized overall accuracy [%]	72.1	71.5	73.5
ϕ coefficient of correspondence	0.44	0.43	0.43

Table 4
Average velocity and the standard deviation simulated by the three tested models

Slope type class	ROCKY1		ROCKY2		ROCKY3	
	Average velocity [m/s]	S.D. [m/s]	Average velocity	S.D.	Average velocity	S.D.
Forest 0–20	30.3	15.3	30.7	15.5	14.9	9.2
Nonforest 0–20	29.8	14.6	31.3	15.0	20.3	9.9
Forest 20–40	27.0	15.0	27.4	15.4	17.8	9.3
Nonforest 20–40	34.3	12.9	35.7	13.4	25.5	10.1
Forest 40–60	17.0	11.4	23.6	12.7	18.7	5.7
Nonforest 40–60	31.6	10.3	33.3	10.7	26.0	8.7
Forest 60–90	27.7	12.3	34.6	10.9	28.6	8.5
Nonforest 60–90	48.4	11.5	50.0	10.7	39.4	8.4

addition, the number of matches between mapped and modelled patterns both on forested and nonforested slopes is determined. To test for the significance of the association between the mapped and modelled patterns of rockfall runout zones, the correspondence coefficient ϕ (Burt and Barber, 1996) is calculated as well.

Furthermore, the rockfall velocities modelled by the three models are compared. For this comparison, different forested and nonforested slope classes are distinguished on the basis of the mean slope gradient.

5. Results

Fig. 6 shows an overview of the general rockfall patterns produced by the three models. They show similar results for ROCKY1 and ROCKY2, with both models producing rockfall areas in the high alpine zones, but none on the forested valley slopes. Results of ROCKY3 contrast sharply with ROCKY1 and ROCKY2 and show rockfall areas on both forested and nonforested slopes throughout the study area.

As shown in Table 3, the percentage of correctly modelled rockfall cells according to the control data varied on forested slopes and nonforested slopes for each model. Moreover, as expected, after examining the general modelled patterns in Fig. 6, there is a large difference among the results of the three models. On forested hillslopes, ROCKY3 performed best, correctly identifying 54.,4% of the mapped rockfall cells, while ROCKY1 and ROCKY2 only modelled 9.5% and 6.3%, respectively, of the mapped rockfall cells. When taking into account both mapped rockfall and nonrockfall cells, the amount of matches increased for ROCKY1 and ROCKY2 to 53.7% and 52.5%, respectively. Again, ROCKY3 performed best in this case, since 66.9% of the modelled cells matched mapped cells.

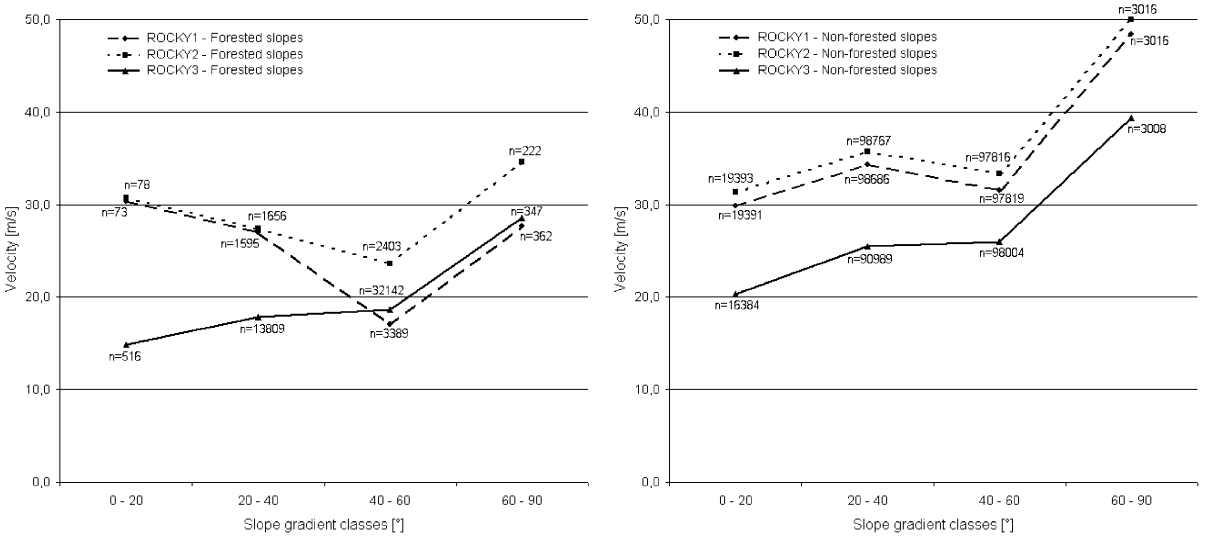

Fig. 7. Summary of the average velocities simulated by ROCKY1, ROCKY2, and ROCKY3 on different forested and nonforested slopes.

Table 5
Contingency tables of ROCKY1 presenting the number of cells and the accuracies normalized for the number of mapped cells

	Mapped as rockfall	Mapped as nonrockfall	Total
Modelled as rockfall	22,737	17,968	40,705
Modelled as nonrockfall	17,720	130,868	148,588
Total	40,457	148,836	189,293
Modelled as rockfall	0.562	0.121	0.683
Modelled as nonrockfall	0.438	0.879	1.317
Total	1.000	1.000	2.000

Table 7
Contingency tables of ROCKY3 presenting the number of cells and the accuracies normalized for the number of mapped cells

	Mapped as rockfall	Mapped as nonrockfall	Total
Modelled as rockfall	26,072	25,980	52,052
Modelled as nonrockfall	14,385	122,856	137,241
Total	40,457	148,836	189,293
Modelled as rockfall	0.644	0.175	0.819
Modelled as nonrockfall	0.356	0.825	1.181
Total	1.000	1.000	2.000

On nonforested slopes, both ROCKY1 and ROCKY2 performed slightly better than ROCKY3. The amount of correctly modelled rockfall cells was 67.4% for ROCKY1 and ROCKY2. For ROCKY3, this amount was 66.8%. Taking into account both mapped rockfall and nonrockfall cells, the produced accuracies are rather equivalent. Table 3 shows that this is also the case for the normalized overall accuracies (normalized for the number of mapped cells) produced by the three models. The highest normalized overall accuracy was, however, produced by ROCKY3 (73.5%). The association between the mapped and modelled patterns of rockfall runout zones, given by the ϕ coefficient in Table 3, is not very strong for all the three models tested ($\phi = 0.44$ or $\phi = 0.43$).

A comparison of the modelled velocities puts forward that the velocity distributions on four mean slope gradient classes, as produced by ROCKY1 and ROCKY2, are rather unrealistic, especially on the forested hillslopes (Table 4 and Fig. 7). On these hillslopes, the average velocity produced by ROCKY1 and ROCKY2 decreased from 27.0 to 17.0 m/s and from 27.4 to 23.6 m/s, respectively, while the mean gradient increased (Fig. 7). ROCKY3 was the only model that produced lower and more realistic velocities (14.9 m/s) on gentle forested hillslopes as well as higher velocities (28.6 m/s) on steep forested hillslopes. On nonforested hillslopes, all the three models produced an increase of velocity with increasing mean slope gradient. However, the velocities produced by ROCKY1 and ROCKY2 were generally 10 m/s higher than those produced by ROCKY3 (Table 4).

Table 6
Contingency tables of ROCKY2 presenting the number of cells and the accuracies normalized for the number of mapped cells

	Mapped as rockfall	Mapped as nonrockfall	Total
Modelled as rockfall	22,179	17,578	39,757
Modelled as nonrockfall	18,278	131,258	149,536
Total	40,457	148,836	189,293
Modelled as rockfall	0.548	0.118	0.666
Modelled as nonrockfall	0.452	0.882	1.334
Total	1.000	1.000	2.000

Despite the low amount of matches on forested hillslopes, ROCKY1 and ROCKY2 produced high normalized overall accuracies. As shown in the contingency tables (Tables 5–7), ROCKY1 and ROCKY2 produced fewer rockfall cells ($n = 40{,}705$ and $n = 39{,}757$, respectively) compared to ROCKY3 ($n = 52{,}052$). As a result, ROCKY1 and ROCKY2 produced more nonrockfall cells ($n = 148{,}588$ and $n = 149{,}536$, respectively) compared to ROCKY3 ($n = 137{,}241$). Therefore, ROCKY1 and ROCKY2 produced accuracies of 0.879 and 0.882 in the nonrockfall class.

The comparison of the amount of both correctly ($n = 26{,}072$) and incorrectly ($n = 25{,}980$) modelled rockfall cells produced by ROCKY3 also provides an interesting result (Table 7). Only 17.5% of all cells mapped as nonrockfall were modelled as rockfall cells. On the other hand, this amount was equal to 49.9% of all the modelled rockfall cells. For ROCKY1 and ROCKY2, this amount was 44.1% and 44.2%, respectively.

6. Discussion

The GIS-based distributed model developed for this study (ROCKY3) simulates motions of falling rocks in detail. This model also incorporates simple forest

parameters (number of trees per hectare and DBH) as well as a module that accounts both for the tree distribution and for the calculation of collisions of rocks against trees. A comparison of the modelled patterns of rockfall runout zones produced by the three models tested (ROCKY1, ROCKY2, and ROCKY3) with mapped rockfall patterns showed that ROCKY3 performed best in simulating rockfall patterns in the study area. In addition, a comparison of the velocities produced by the three models showed that ROCKY3 simulates rockfall velocities more accurately on both forested and nonforested hillslopes. Unfortunately, no data are currently available on rockfall velocities within the study area. However, during real-time rockfall experiments in the French Alps, on a nonforested avalanche track on a talus slope with a mean slope gradient of approximately 38°, falling rocks reached maximum velocities of 25 m/s (F. Berger-Cemagref Grenoble, personal communication). These slopes are typical rockfall-endangered areas that are also found in our study area. ROCKY1 and ROCKY2 generally produced higher velocities on less steep forested and nonforested hillslopes. In contrast, the velocities produced by ROCKY3 on similar hillslopes corresponded with this observation.

Although ROCKY3 provided better overall results than ROCKY1 and ROCKY2, all three models produced similar normalized overall accuracies. Since ROCKY1 and ROCKY2 simulated fewer rockfall cells than ROCKY3, the probability of cells being modelled incorrectly (mismatch with cells mapped as nonrockfall) decreased. In addition, 80% of the mapped cells are nonrockfall areas. Therefore, the amount of nonrockfall matches was very high for ROCKY1 and ROCKY2. As a consequence, the normalized overall accuracy was also high.

The three models tested encountered similar problems regarding mismatches between modelled rockfall cells and mapped nonrockfall cells (ROCKY3: 49.9%, ROCKY1: 44.1%, and ROCKY2: 44.2%). These mismatches were mainly caused by the input data, being GIS rasters with a support of 25 × 25 m. Within such rasters, fine-scale variation in the mean slope gradient and surface cover characteristics as observed in the field is lost. In addition, the topography as shown by a DEM with a support of 25 × 25 m is much smoother than the real topography (Hodgson, 1995; Walker and Willgoose, 1999; Yin and Wang, 1999; Zhang et al., 1999; Schoorl et al., 2000).

To account for this smoothing effect, starting locations in rockfall source cells are set at 10 m above the surface, since it was observed in the study area that small cliff faces with a height of 10–50 m do occur on hillslopes that are represented by raster cells with a slope gradient of 40°. Due to the use of the simple threshold value for identifying the rockfall source cells, the model produced some rockfall areas in locations where this is not the case in reality. Therefore, the model results probably improve considerably if these small cliff faces could be identified for the whole study area, which is a GIS research challenge.

The use of a mean slope gradient threshold of 40° for rockfall source areas also had a distinct effect on the modelled velocities. The velocity graph (Fig. 7) shows that the average velocities produced by the three models only increase slightly or even decrease between the slope classes 20–40° and 40–60°. This may be explained by two reasons. Firstly, since the threshold value for rockfall source areas was defined as 40°, the model started to simulate rockfall in cells with a mean slope gradient equal to or steeper than 40°. Depending on the friction or the restitution coefficients, the simulated rock stopped within the source cell, or accelerated and consequently shifted to the next cell in the falltrack. The latter generally occurred in cells with a mean slope angle much steeper than 40°. Acceleration also occurred on slopes with a mean slope gradient of 40°, but the resulting velocity in those source cells was not as high as in source cells with steeper slope gradients. Secondly, the low velocities in cells with a mean slope gradient of around 40° could be the result of falling rocks that were simulated from source cells upslope with slope gradients slightly steeper than 40°. Downslope, the velocity and the mean gradient of the slope decreased and, consequently, the rock could stop in one of the downslope cells, which could have a slope gradient of approximately 40°. High velocities on slopes with mean gradients much lower than 40° may be explained by the fact that these cells were mainly runout zones of falling rocks simulated from steep to very steep (>60°) source cells. These observations show that the threshold of 40° is a safe value to account for the smoothing effect of the 25 × 25-m

DEM, but it might also lead to incorrectly modelled patterns of rockfall runout zones.

The use of a falltrack calculation based on a multiple flow algorithm (Quinn et al., 1991; Wolock and McCabe, 1995) would improve the model as well. The currently used falltrack calculation will always generate converging rockfall runout zones instead of diverging zones (e.g., as observed on talus cones in the field). The multiple flow algorithm enables modelling of more realistic rockfall accumulation areas, which might improve the number of matches between model and map. Within this study, it was chosen to test the models with a simple falltrack procedure because this facilitated the comparison of the model results. The incorporation of the multiple flow algorithm in the three models tested would introduce a stochastic factor and therefore more difficulties for comparing the results.

The friction coefficient, the tangential restitution coefficient, and the normal restitution coefficient for different land-cover classes were estimated from literature data on the basis of the land-cover map. Firstly, this was done because field data were not available and, secondly, because simulation errors were interpreted as model errors rather than parameter estimation errors. The latter enabled us to compare the three models on their ability to predict rockfall runout zones on slopes with different characteristics throughout the study area.

As shown by the accuracy of the modelled patterns of rockfall runout zones on nonforested hillslopes as produced by the three models, the estimation of parameter values worked satisfactory. However, a more objective method for estimating these parameters at a regional scale would be preferred. Regarding the effect of forests on patterns of rockfall runout zones, different forest densities could be described reasonably well by using the number of trees per hectare and the DBH, but incorporating gaps within forest stands was not possible. Gaps in a forest are important elements of a forest structure that determine the level of protection a mountain forest provides against rockfall (Bebi et al., 2001). For rockfall modelling at a regional scale, there is thus a need for both an automated assessment and a model representation of gaps in mountain forests at a regional scale. Gaps within forests could, for example, be represented in a model by using a fractal dimension (Xu and Lanthrop, 1995). In this case, mountain forests are considered as porous systems in which the fractal dimension of the pore space represents the gap distribution. For example, such an approach has been used for describing pore structures of Swiss cheese models (Klemm et al., 1999).

7. Conclusions

From all the three models tested in this study, the combination of a GIS-based model and a process-based model, which simulates the motion of falling rocks in detail and incorporates simple forest stand parameters, was most accurate in predicting patterns of rockfall runout zones at a regional scale. Like all the models tested, this model combines three main procedures: the identification of source areas, the determination of falltracks, and the calculation of the rockfall runout zones.

Regarding the identification of source areas, the model probably improves considerably if rockfall source areas, such as small cliff faces, could be identified in detail, instead of using a mean slope gradient threshold value. With respect to determining the falltrack, the use of a multiple flow algorithm could also improve the model. The calculation of the rockfall runout zones was satisfactory. However, gaps within forest stands were not taken into account in the input data. Incorporating gaps in the forest input data might result in a better representation of the velocity development on forested slopes. Therefore, a better representation of gaps within forest stands at a regional scale is needed.

Acknowledgements

We gratefully acknowledge Bernhard Maier for providing the forest inventory data and for sharing his knowledge of mountain forest management. Furthermore, we wish to thank Ger Bergkamp and Anton Imeson for their suggestions for improvement.

References

Azzoni, A., Barbera, G.L., Zaninetti, A., 1995. Analysis and prediction of rockfalls using a mathematical model. International Journal of Rock Mechanics and Mining Science 32, 709–724.

Bebi, P., Kienast, F., Schönenberger, W., 2001. Assessing structures in mountain forests as a basis for investigating the forests' dynamics and protective function. Forest Ecology and Management 145, 3–14.

BEV, 2001. Bundesamt für Eich-und Vermessungswesen, Produktinformation zum Geländehöhenmodell. http://www.bev.gv.at/.

Bozzolo, D., Pamini, R., 1986. Simulation of rock falls down a valley side. Acta Mechanica 63, 113–130.

Burt, J.E., Barber, G.M., 1996. Elementary Statistics for Geographers. Guilford Press, New York. 640 pp.

Chau, K.T., Wong, R.H.C., Lee, C.F., 1998. Rockfall problems in Hong Kong and some new experimental results for coefficient of restitution. International Journal of Rock Mechanics and Mining Science 35 (4), 662–663.

Chau, K.T., Wong, R.H.C., Wu, J.J., 2002. Coefficient of restitution and rotational motions of rockfall impacts. International Journal of Rock Mechanics and Mining Sciences 39 (1), 69–77.

De Graaff, L.W.S., de Jong, M.G.G., Rupke, J., Verhofstad, J., 1987. A geomorphological mapping system at scale 1,10.000 for mountainous areas. Zeitschrift für Geomorphologie N.F. 31 (2), 229–242.

Dorren, L.K.A., 2003. A review of rockfall mechanics and modelling approaches. Progress in Physical Geography 27 (1), 69–87.

Dorren, L.K.A., Maier, B., Seijmonsbergen, A.C., in press. Improved Landsat-based forest mapping in steep mountainous terrain using object-based classification. Forest Ecology and Management.

ESRI, 2002. Arcview 3.2 and Spatial Analyst. Environmental Systems Research Institute. http://www.esri.com.

GBA, 1998. In: Oberhauser, R., Rataj, W. (Eds.), Geologisch-Tektonische Übersichtskarte von Vorarlberg (1,200,000) with Erläuterungen. Geological Survey of Austria, Vienna, Austria.

Giani, G.P., 1992. Rock Slope Stability Analysis. Balkema, Rotterdam. 361 pp.

GSC, 2002. GSC Atlantic Rock Properties Database. Geological Survey of Canada/Dalhousie University. http://gsca.nrcan.gc.ca/pubprod/rockprop/search_e.php.

Hodgson, M.E., 1995. What cell-size does the computed slope aspect angle represent. Photogrammetric Engineering and Remote Sensing 61 (5), 513–517.

Jenson, S.K., Domingue, J.O., 1988. Extracting topographic structure from digital elevation data for geographic information system analysis. Photogrammetric Engineering and Remote Sensing 54 (11), 1593–1600.

Keller, M., 1994. Considerations to quantify forest functions by means of a GIS. Proceedings EGIS '94, Fifth European Conference and Exhibition on Geographical Information Systems, Utrecht. EGIS Foundation, vol. 1, pp. 1676–1681.

Kirkby, M.J., Statham, I., 1975. Surface stone movement and scree formation. Journal of Geology 83, 349–362.

Klemm, A., Müller, H.-P., Kimmich, R., 1999. Evaluation of fractal parameters of percolation model objects and natural porous media by means of NMR microscopy. Physica A 266, 242–246.

Kobayashi, Y., Harp, E.L., Kagawa, T., 1990. Simulation of rockfalls triggered by earthquakes. Rock Mechanics and Rock Engineering 23, 1–20.

Köppen, W., 1918. Klassifikation der Klimate nach Temperatur, Niederschlag, und Jahreslauf. Petermann's Mitteilungen 64, 193–203.

Kräuchi, N., Brang, P., Schönenberger, W., 2000. Forests of mountainous regions, gaps in knowledge and research needs. Forest Ecology and Management 132, 73–82.

Maier, B., 1993. Forstinventur Stand Montafon. Internal Report. Stand Montafon, Schruns. 154 pp.

Mathworks, 2002. Matlab, the language of technical computing, version 5.3. The MathWorks. http//www.mathworks.com.

Meißl, G., 1998. Modellierung der Reichweite von Felsstürzen. Fallbeispeile zur GIS-gestützten Gefahrenbeurteilung aus dem Beierischen und Tiroler Alpenraum. Innsbrucker Geografischen Studien 28. PhD Thesis, Universität Innsbruck, Innsbruck, Austria. 249 pp.

Meißl, G., 2001. Modelling the runout distances of rockfalls using a geographic information system. Zeitschrift für Geomorphologie N.F. Supplementband 125, 129–137.

Motta, R., Haudemand, J.C., 2000. Protective forests and silvicultural stability—an example of planning in the Aosta Valley. Mountain Research and Development 20 (2), 180–187.

Okura, Y., Kitahara, H., Sammori, T., Kawanami, A., 2000. The effects of rockfall volume on runout distance. Engineering Geology 58 (2), 109–124.

Pfeiffer, T.J., Bowen, T.D., 1989. Computer simulation of rockfalls. Bulletin of the Association of Engineering Geologists 26 (1), 135–146.

Quinn, P., Beven, K., Chevallier, P., Planchon, O., 1991. The prediction of hillslope flow paths for distributed hydrological modelling using digital terrain models. Hydrological Processes 5, 59–79.

Scheidegger, A.E., 1975. Physical Aspects of Natural Catastrophes. Elsevier, Amsterdam.

Schoorl, J.M., Sonneveld, M.P.W., Veldkamp, A., 2000. Three-dimensional landscape process modelling: the effect of DEM resolution. Earth Surface Processes and Landforms 25, 1025–1034.

Seijmonsbergen, A.C., 1992. Geomorphological evolution of an alpine area and its application to geotechnical and natural hazard appraisal in the NW. Rätikon and S. Walgau (Vorarlberg, Austria), including map series at 1,10,000 scale. PhD Thesis, University of Amsterdam, Amsterdam, the Netherlands. 109 pp.

Statham, I., Francis, S.C., 1986. Influence of scree accumulation and weathering on the development of steep mountain slopes. In: Abrahams, A.D. (Ed.), Hillslope Processes. Allen and Unwin, Winchester, pp. 245–267.

van Dijke, J.J., van Westen, C.J., 1990. Rockfall hazard, a geomorphological application of neighbourhood analysis with ILWIS. ITC Journal 1, 40–44.

van Noord, H., 1996. The role of geomorphological information in ecological forest site typology in mountainous areas, a methodological study in the E-Rätikon and NW-Montafon mountains (Vorarlberg, Austria). PhD Thesis, University of Amsterdam, Amsterdam, the Netherlands. 185 pp.

Walker, J.P., Willgoose, G.R., 1999. On the effect of digital elevation model accuracy on hydrology and geomorphology. Water Resources Research 35 (7), 2259–2268.

Wolock, D.M., McCabe Jr., G.J., 1995. Comparison of single and

multiple flow direction algorithms for computing topographic parameters in TOPMODEL. Water Resources Research 31, 1315–1324.

Xu, J., Lanthrop, R.G., 1995. Improving simulation accuracy of spread phenomena in a raster-based Geographic Information System. International Journal of Geographical Information Systems 9 (2), 153–168.

Yin, Z.Y., Wang, X.H., 1999. A cross-scale comparison of drainage basin characteristics derived from digital elevation models. Earth Surface Processes and Landforms 24, 557–562.

Zevenbergen, L.W., Thorne, C.R., 1987. Quantitative analysis of land surface topography. Earth Surface Processes and Landforms 12, 47–56.

Zhang, X.Y., Drake, N.A., Wainwright, J., 1999. Comparison of slope estimates from low resolution DEMs: scaling issues and a fractal method for their solution. Earth Surface Processes and Landforms 24, 763–779.